

Transitions in pedestrian fundamental diagrams of straight corridors and T-junctions

J Zhang¹, W Klingsch¹, A Schadschneider² and A Seyfried^{3,4}

¹ Institute for Building Material Technology and Fire Safety Science, Bergische Universität Wuppertal, Pauluskirchstrasse 11, 42285 Wuppertal, Germany

² Institut für Theoretische Physik, Universität zu Köln, 50937 Köln, Germany

³ Computer Simulation for Fire Safety and Pedestrian Traffic, Bergische Universität Wuppertal, Pauluskirchstrasse 11, 42285 Wuppertal, Germany

⁴ Jülich Supercomputing Centre, Forschungszentrum Jülich GmbH, 52425 Jülich, Germany

E-mail: jun.zhang@uni-wuppertal.de, klingsch@uni-wuppertal.de, as@thp.uni-koeln.de, seyfried@uni-wuppertal.de

Abstract. Many observations of pedestrian dynamics, including various self-organization phenomena, have been reproduced successfully by different models. But the empirical databases for quantitative calibration is still insufficient, e.g. the fundamental diagram as one of the most important relationships displays non-negligible differences among various studies. To improve this situation, experiments in straight corridors and T-junction are performed. Four different measurement methods are defined to study their effects on the fundamental diagram. It is shown that they have minor influences for $\rho < 3.5 \text{ m}^{-2}$ but only the Voronoi method is able to resolve the fine-structure of the fundamental diagram. This enhanced measurement method permits to observe the occurrence of boundary-induced phase transition. For corridors of different widths we found that the specific flow concept works well for $\rho < 3.5 \text{ m}^{-2}$. Moreover, we illustrate the discrepancies between the fundamental diagrams of a T-junction and a straight corridor.

1. Introduction

During the last few decades, research on pedestrian and traffic flow became popular and attracted a lot of attention [1, 2, 3, 4, 5, 6]. The investigation of pedestrian motion plays an important role in guaranteeing the safety of pedestrians in complex buildings or at mass events. A large number of models have been developed in the past. Most of them are able to reproduce phenomena of pedestrian movement qualitatively. Before using a model to predict quantitative results like the total evacuation time, it needs to be calibrated thoroughly and quantitatively using empirical data. However, this is still difficult due to a lack of reliable experimental data. In addition, the small number of available datasets shows surprisingly large differences [7, 8].

In recent years, several well-controlled pedestrian experiments [9, 10, 11, 12, 13] and field studies [14, 15, 16] have been performed. One of the most important characteristics of pedestrian dynamics is the fundamental diagram which states the relationship between

pedestrian flow and density. Several researchers, in particular Fruin and Pauls [17], Predtechenskii and Milinskii [18], Weidmann [19], Helbing et al. [20] have collected information about the relation of occupants density and velocity. But there exists considerable disagreement among these data. In the comparison performed in [21] the density ρ_0 , where the velocity approaches zero due to overcrowding, ranges from 3.8 m^{-2} to 10 m^{-2} , while the density ρ_c where the flow reaches its maximum ranges from 1.75 m^{-2} to 7 m^{-2} . Several explanations for these discrepancies have been proposed, including cultural factors [22], differences between unidirectional and multidirectional flow [23, 24].

For single-file movements it was found that even the measurement method has a large influence on the fundamental diagram and could be responsible for the observed deviations [21]. For identical facilities (e.g., corridors, stairs, doors) with different width it is usually assumed that the fundamental diagrams are unified in a single diagram for specific flow J_s . The study of Hankin et al. [25] in the London subway shows that above a certain minimum of about four feet the maximum flow in subway stations is directly proportional to the width of the corridor. Besides, it is still not clear whether or not the fundamental diagrams for other scenarios like bottlenecks or T-junctions are the same.

Facing such questions, a series of well-controlled laboratory experiments are carried out. The goals of this study are to improve the database related to pedestrian dynamics, to determine the influence of measurement methods on the fundamental diagram, and to check whether or not the fundamental diagram for different types of facilities can be unified in a single diagram.

In section 2, the experiment setup will be briefly described. The measurement methods used in this paper are introduced and defined in section 3. The main results of the work are in section 4. Finally, we make some concluding remarks in section 5.

2. Experiment Setup

The experiments were performed in hall 2 of the fairground Düsseldorf (Germany) in May 2009. They are part of the Hermes project [26] in which the data resulting from the experiments will be used to calibrate and test pedestrian movement models. The experiments were conducted with up to 350 participants. They were composed mostly of students and each of them was paid 50 € per day. The mean age and height of the participants were 25 ± 5.7 years and 1.76 ± 0.09 m, respectively. The free velocity $v_0 = 1.55 \pm 0.18$ m/s was obtained by measuring 42 participants' free movement.

Figure 1 shows the sketches of the setups and some snapshots during the experiments. Two types of geometries, straight corridor (C) and T-junction (T), were used in the experiment. 28 runs (see Table 2) were performed in straight corridors with widths of 1.8 m, 2.4 m and 3.0 m respectively. 7 runs for the T-junction with corridor width of 2.4 m were carried out (see Table 3). To regulate the pedestrian density in the corridor, the width of the entrance b_{entrance} and the exit b_{exit} was changed in each run. For details, see Figure 1, Table 2 and 3. At the beginning, the participants were held within a waiting area. Equal densities for different runs were arranged by partitioning the waiting area and counting the number of

people in the parts. Standing at the waiting area, they pass through a 4 m passage into the corridor. The passage was used as a buffer to minimize the effect of the entrance. In this way, the pedestrian flow in the corridor was nearly homogeneous over its entire width. When a pedestrian leaves through an exit, he or she returns to the waiting area for the next run.

The experiments were recorded by two cameras mounted at the rack of the ceiling of the hall. To cover the complete region, the left and the right part of the corridor were recorded by the two cameras separately. The pedestrian trajectories were automatically extracted from video recordings using the software *PeTrack* [27]. Finally, the trajectory data from the two cameras were corrected manually and combined automatically. The frame rate of the trajectory data corresponds to 16 fps. Figure 2 shows the trajectories of the head of each pedestrian in two runs of the experiment. From these trajectories, pedestrian characteristics including flow, density and velocity are determined.

3. Measurement Methods

For vehicular traffic it is well known that different measurement methods lead to different fundamental diagrams [28, 29]. The results presented in [21] using pedestrian trajectories of single file movement, have also shown how large variations induced by different measurement methods could be. In previous studies of pedestrian streams, different measurement methods were used limiting the comparability of the data. E.G. Helbing et al. proposed a Gaussian, distance-dependent weight function [20] to measure the local density and local velocity. Predtechenskii and Milinskii [18] used a dimensionless definition to consider different body sizes and Fruin introduced the "Pedestrian Area Module" [17]. All of these definitions have their advantages and disadvantages. To analyze all of them goes beyond the scope of this paper. To enable a detailed analysis, we study the influence of several measurement methods on the fundamental diagram and analyze which methods lead to the smallest fluctuations.

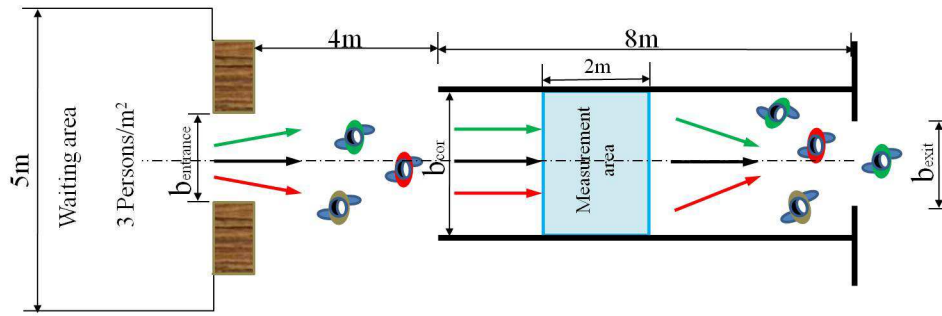
In this study four measurement methods were used to calculate the basic quantities: flow, density and velocity. Some terminologies used here are taken from [21] and [30].

3.1. Method A

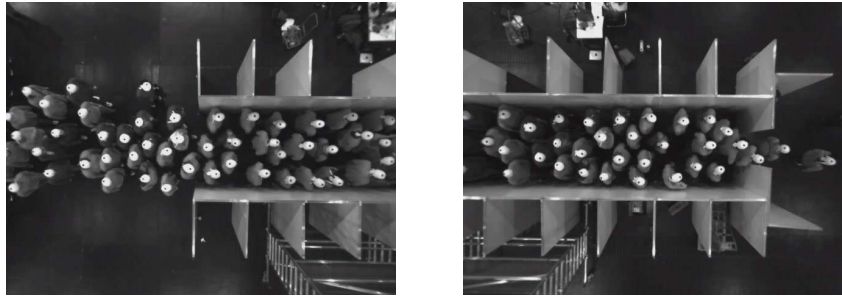
Method A calculates mean value of flow and density over time. A reference location x in the corridor is taken and studied over a fixed period of time Δt (as shown in Figure 3). We refer to this average by $\langle \rangle_{\Delta t}$. Using this method we can obtain the pedestrian flow J and the velocity v_i of each pedestrian passing x directly. Thus, the flow over time $\langle J \rangle_{\Delta t}$ and the time mean velocity $\langle v \rangle_{\Delta t}$ can be calculated as

$$\langle J \rangle_{\Delta t} = \frac{N_{\Delta t}}{t_{N_{\Delta t}}} \quad \text{and} \quad \langle v \rangle_{\Delta t} = \frac{1}{N_{\Delta t}} \sum_{i=1}^{N_{\Delta t}} v_i(t) \quad (1)$$

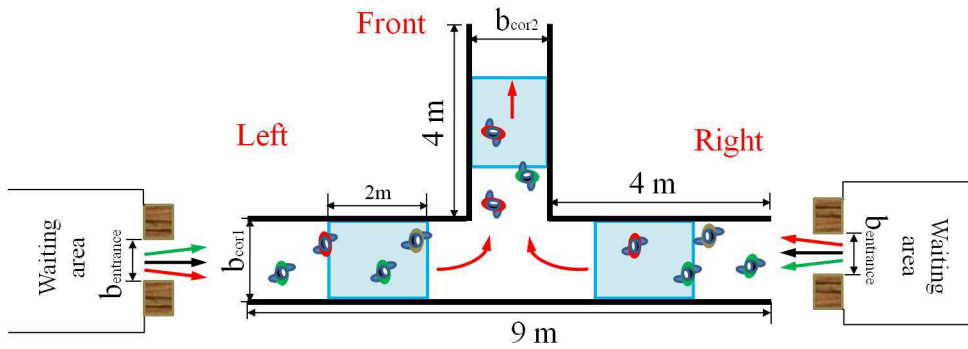
where $N_{\Delta t}$ is the number of persons passing the location x during the time interval Δt . $t_{N_{\Delta t}}$ is the time between the first and the last of the $N_{\Delta t}$ pedestrians. Thus $t_{N_{\Delta t}}$ is the actual time that the $N_{\Delta t}$ pedestrians used for passing the location. It can be different from Δt . The time mean velocity $\langle v \rangle_{\Delta t}$ is defined as the mean value of the instantaneous velocities $v_i(t)$ of the $N_{\Delta t}$



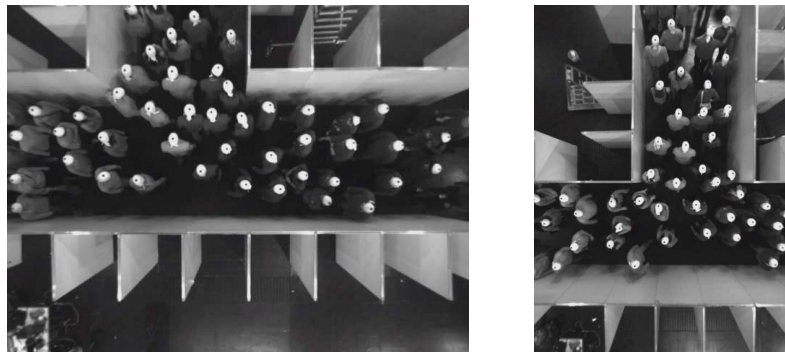
(a) Sketch of experiment at straight corridor



(b) Snapshots from experiment C-180-180-070

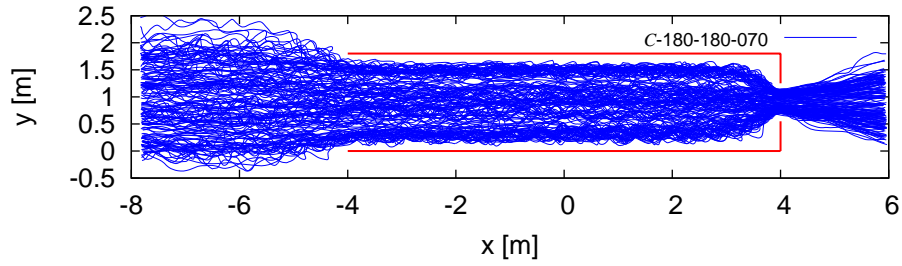


(c) Sketch of experiment at T-junction

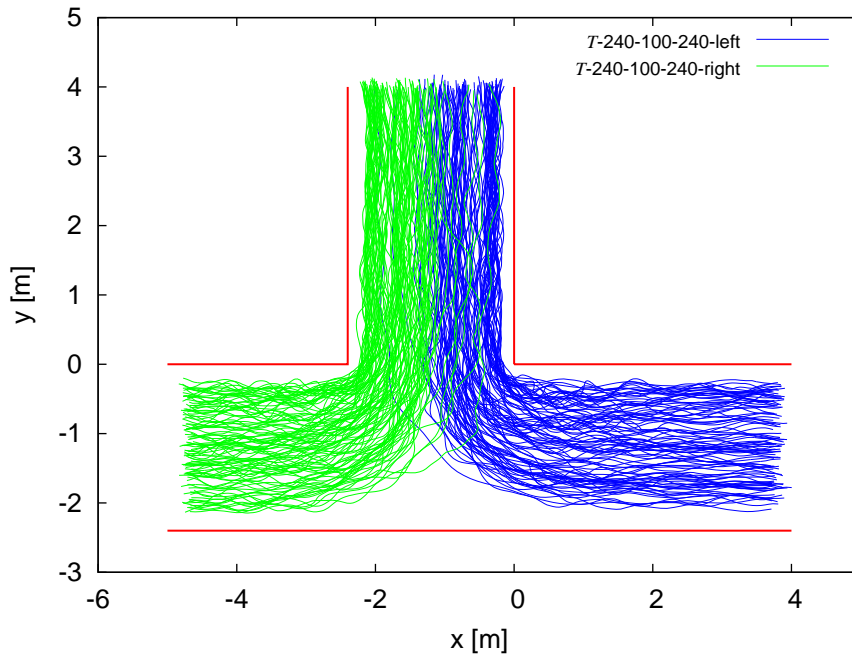


(d) Snapshots from experiment T-240-120-240

Figure 1. Sketch of the experimental setup ((a) and (c)) and snapshots of the experiment from the two cameras respectively ((b) and (d)). The shaded regions in (a) and (c) are the chosen measurement areas with 2 m in length.



(a) C-180-180-070



(b) T-240-100-240

Figure 2. The trajectories for all pedestrians in the experiment. The data are extracted from the video recording by the free software *PeTrack* [27].

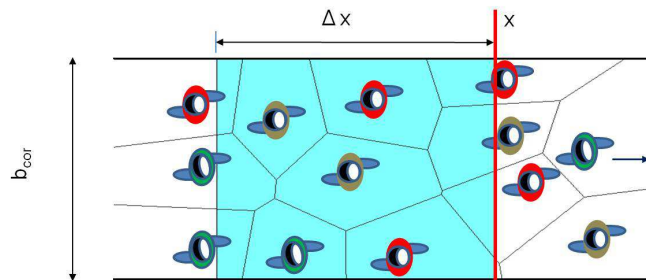


Figure 3. Illustration of different measurement methods. *Method A* is a kind of local measurement at cross-section with position x averaged over a time interval Δt , while *Methods B–D* measure at a certain time and average the results over space Δx . Note that for *Method D*, the Voronoi diagrams are generated according to the spatial distributions of pedestrians frame by frame.

persons according to equation (2). We calculate $v_i(t)$ by use of the displacement of pedestrian i in a small time interval $\Delta t'$ around t :

$$v_i(t) = \frac{x_i(t + \Delta t'/2) - x_i(t - \Delta t'/2)}{\Delta t'} \quad (2)$$

3.2. Method B

The second method measures the mean value of velocity and density over space and time. The spatial mean velocity and density are calculated by taking a segment Δx in the corridor as the measurement area. The velocity $\langle v \rangle_i$ of each person is defined as the length Δx of the measurement area divided by the time he or she needs to cross the area (see equation (3)),

$$\langle v \rangle_i = \frac{\Delta x}{t_{\text{out}} - t_{\text{in}}} \quad (3)$$

where t_{in} and t_{out} are the times a person enters and exits the measurement area, respectively. The density ρ_i for each person is calculated with equation (4):

$$\langle \rho \rangle_i = \frac{1}{t_{\text{out}} - t_{\text{in}}} \cdot \int_{t_{\text{in}}}^{t_{\text{out}}} \frac{N'(t)}{b_{\text{cor}} \cdot \Delta x} dt \quad (4)$$

b_{cor} is the width of the measurement area while $N'(t)$ is the number of person in this area at a time t .

3.3. Method C

The third measurement method is the classical method. The density $\langle \rho \rangle_{\Delta x}$ is defined as the number of pedestrians divided by the area of the measurement section:

$$\langle \rho \rangle_{\Delta x} = \frac{N}{b_{\text{cor}} \cdot \Delta x} \quad (5)$$

The spatial mean velocity is the average of the instantaneous velocities $v_i(t)$ for all pedestrians in the measurement area at time t :

$$\langle v \rangle_{\Delta x} = \frac{1}{N} \sum_{i=1}^N v_i(t) \quad (6)$$

3.4. Method D

This method is based on the use of Voronoi diagrams [31] which are a special kind of decomposition of a metric space determined by distances to a specified discrete set of objects in the space. At any time the positions of the pedestrians can be represented as a set of points, from which the Voronoi diagram (see Figure 3) can be generated. The Voronoi cell area, A_i , for each person i can be obtained. Then, the density and velocity distribution of the space ρ_{xy} and v_{xy} can be defined as

$$\rho_{xy} = 1/A_i \quad \text{and} \quad v_{xy} = v_i(t) \quad \text{if } (x, y) \in A_i \quad (7)$$

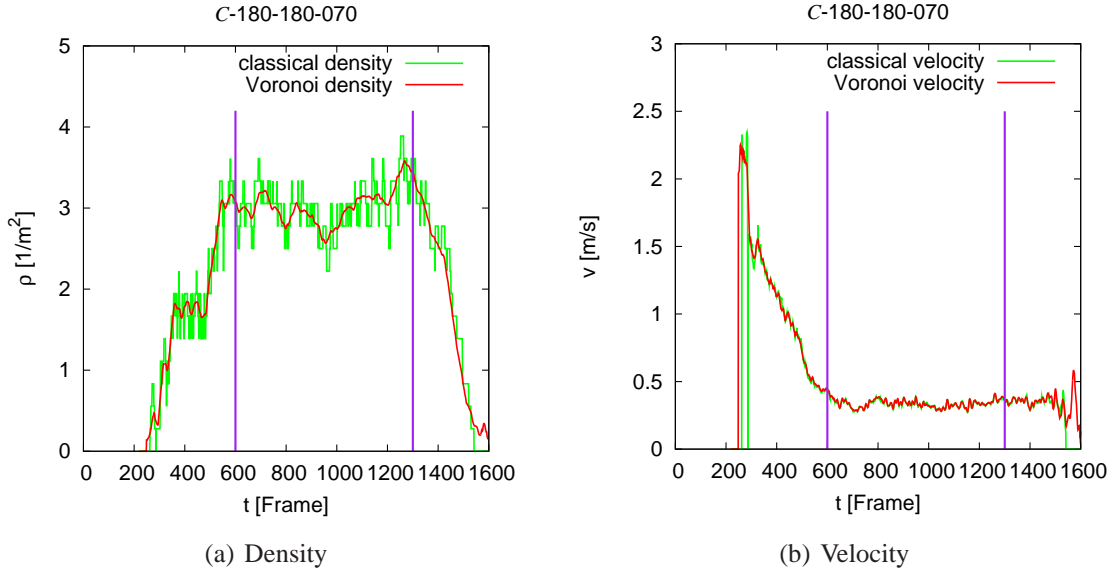


Figure 4. Time series of density and velocity using Method *C* and *D*. The two vertical lines indicate the beginning and the end of stationary states.

where $v_i(t)$ is the instantaneous velocity of each person, see equation (2). The Voronoi density and velocity for the measurement area is defined as [30]

$$\langle \rho \rangle_v = \frac{\iint \rho_{xy} dx dy}{b_{\text{cor}} \cdot \Delta x} \quad (8)$$

$$\langle v \rangle_v = \frac{\iint v_{xy} dx dy}{b_{\text{cor}} \cdot \Delta x} \quad (9)$$

4. Results

We calculate the fundamental diagram for the straight corridor experiments using the methods introduced in the last section. To facilitate a comparison among these four methods, we use the hydrodynamic flow equation $J = \rho v b$.

4.1. Influence of the measurement method

For *Method A* we choose the time interval $\Delta t = 10$ s, $\Delta t' = 0.625$ s (corresponding to 10 frames) and the measurement position at $x = 0$ (see Figure 2). For the other three methods a rectangle with length 2 m from $x = -2$ m to $x = 0$ and width of the corridor is chosen as the measurement area. We calculate the densities and velocities every frame with a frame rate of 16 fps. All data below are obtained from the trajectories. To determine the fundamental diagram only data at stationary states, which were selected manually by analyzing the time series density and velocity (see Figure 4), were used. For *Method D* we use one frame per second to decrease the number of data points and to represent the data more clearly.

Figure 5 shows the relationship between density and velocity obtained from different methods. Using *Method A* the flow and mean velocity can be obtained directly. To get the

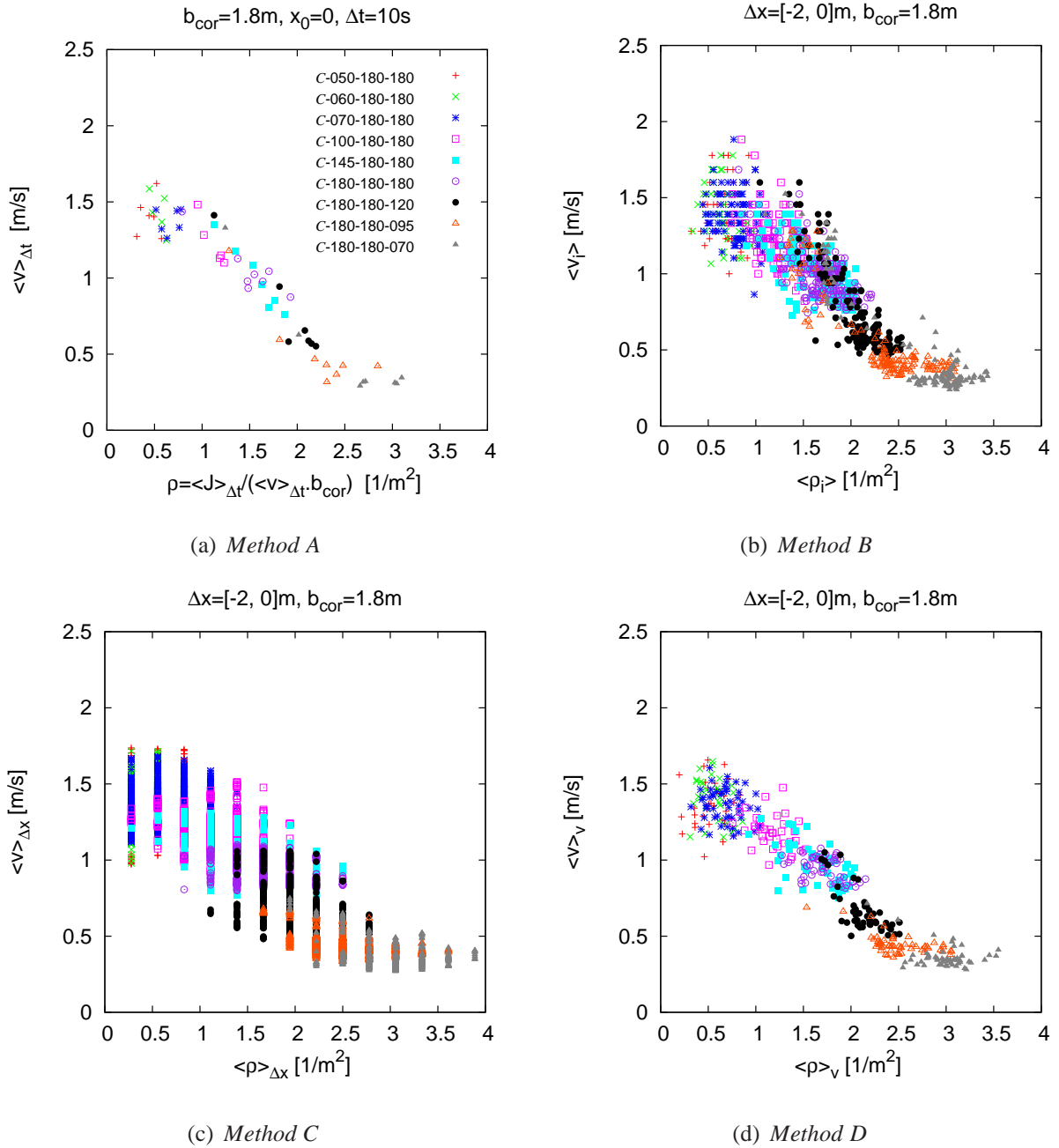


Figure 5. The fundamental diagrams, the relationship between density and velocity, measured on the same set of trajectories but with different methods. Except for the density in (a), which is calculated using $\rho = J/(b \cdot \Delta x)$, all data are determined directly from the trajectories. The legends in (b), (c) and (d) are the same as in (a).

relationship between density and flow, the equation $\rho = \langle J \rangle_{\Delta t} / (\langle v \rangle_{\Delta t} \cdot b_{\text{cor}})$ was adopted to calculate the density. For the *Method B*, *C* and *D* the mean density and velocity can be obtained directly since they are mean values over space. There exists a similar trend of the fundamental diagram obtained using the different methods. However, their influence on the scatter of the results is obvious. Table 1 shows the standard deviation of velocities in certain density intervals for different measurement methods. Compared to the other approaches, the fluctuations in *Method B* and *C* are larger.

Another criterion for the quality of the methods is the resolution in time and space. Even if *Method A* provides a smaller standard deviation than *Method D*, the low resolution in time smears the transition at $\rho = 2\text{m}^{-2}$ clearly visible in Figure 5(d). The density in *Method C* has a strong dependence on the size of the measurement area $A_m = b_{\text{cor}} \cdot \Delta x$. The interval between two density values is $1/A_m$, which indicates that the measurement area should not be too small using this method. But large areas can not provide a detailed spatial resolution. *Method D* can reduce the density and velocity scatter [30]. The reduced fluctuation of *Method D* is combined with a good resolution in time and space, which reveal a phenomenon that is not observable with *Method A*, *B* and *C*. In Figure 5(d) it seems that there is a discontinuity of the fundamental diagram when the density is about 2m^{-2} . This will be analyzed in detail in section 4.3.

Figure 6 shows the relationship between the density and flow obtained from different methods. The pedestrian flow shows small fluctuations at low densities and high fluctuations at high densities. The fluctuations for *Method A* and *Method D* are smaller than that for other methods. However, there is a major difference between the results. While the fundamental diagrams obtained using *Method A* and *Method C* are smooth, fundamental diagrams obtained with *Method B* and *Method D* show a clear discontinuity at a density of about 2m^{-2} . The average over a time interval of *Method A* and the large scatter of *Method C* blur this discontinuity. In disagreement with the results in [21], no marked differences occur among the fundamental diagrams produced by different methods (see Figure 5). In [21], single-file movement in a corridor with periodic boundary was studied. In that experiment, distinct stop waves occurred at high densities and lead to large inhomogeneities in the trajectories. Possibly the differences of different methods will be larger in the cases where stop waves occur or when the characteristic of the pedestrian flow is not laminar.

Table 1. Standard deviation of velocities in certain density interval for different methods

Density interval [m^{-2}]	<i>Method A</i> [m/s]	<i>Method B</i> [m/s]	<i>Method C</i> [m/s]	<i>Method D</i> [m/s]
$\rho \in [0.8, 1.2]$	0.119	0.169	0.175	0.120
$\rho \in [1.6, 2.0]$	0.086	0.144	0.175	0.111

4.2. Influence of the corridor width

From the above analysis it can be concluded that there is no large influence of different methods on the results for the density region without the stop wave phenomenon. We have

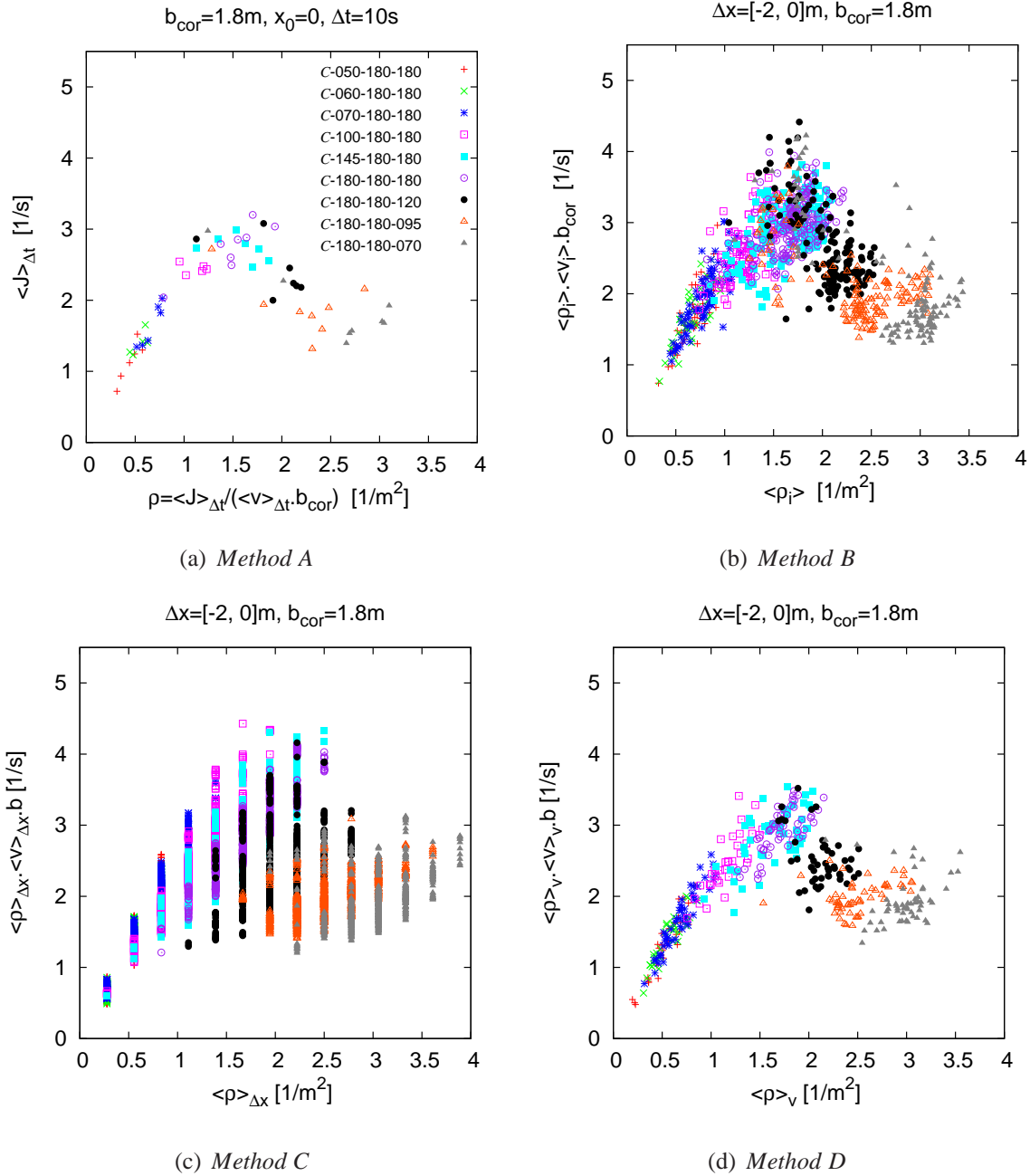


Figure 6. The fundamental diagrams, the relationship between density and flow, measured at the same set of trajectories but with different methods. The density in (a) is calculated indirectly using $\rho = J / (b \cdot \Delta x)$, while the flows in (b), (c) and (d) are obtained by adopting the equation $J = \rho v b$. The legends in (b), (c) and (d) are the same as in (a).

shown that the results with the smallest fluctuations are provided by *Method A* and *D*. Thus we analyze the other unidirectional experiments with corridor width 2.4 m and 3.0 m using *Method A* and *Method D*.

Figure 7 shows the relationship between density, velocity and flow using these two methods. The fundamental diagram of the same type of corridor but with different widths are compared. The fundamental diagrams for these three widths agree well for both methods. This result is in conformance with Hankin's findings [25]. He found that above a certain minimum of about 4 ft (about 1.22 m) the maximum flow in subways is directly proportional to the width of the corridor. Our results agree with the assumption that the specific flow $J_s = J/b$ is independent of the width of the facility. However, it is possible that for small corridors or very high densities J_s becomes dependent on b .

4.3. Discontinuous trend of the fundamental diagram

In Figure 5(b) and 5(d) a discontinuity occurs at $\rho \approx 2 \text{ m}^{-2}$, separating the function $J_s(\rho)$ in a region $\rho < 2 \text{ m}^{-2}$ with negative curvature and a region $\rho > 2 \text{ m}^{-2}$ with positive curvature. Moreover, for *Method D* a gap occurs around $v = 0.7 \text{ m/s}$. This transition is also found in the experiments with $b_{\text{cor}} = 2.4 \text{ m}$ and $b_{\text{cor}} = 3.0 \text{ m}$. The fundamental diagram changes qualitatively when the width b_{exit} of the exit is modified. The modification of the exit width was necessary to achieve high densities. However, it seems that this slight change in the experimental setup causes a significant change in the flow-density relation. This point becomes obvious in the velocity-density relation, especially in Figure 5(d) which is obtained from *Method D*. Although the measurement area in the corridor is 4 m away from the exit, the influence of the change of the exit on the fundamental diagram is sensitive. The decreasing of the exit width limits the outflow of pedestrians and leads to a discontinuity in the fundamental diagram. This can be interpreted in terms of the well-established theory of boundary induced phase transitions, see section 4.4.

4.4. Interpretation in terms of boundary-induced phase transitions

Some of the results can be interpreted in terms of the well-established theory of boundary-induced phase transitions [6, 32]. In nonequilibrium systems phase transitions (in the bulk) can be induced by changing boundary conditions, generically input and output rates in the case of transport systems. A mesoscopic theory has been developed which allows to derive the phase diagram of an open system (allowing input and output of particles at the boundaries, see Figure 8) from the fundamental diagram of the periodic system [33]. This theory even makes quantitative predictions on the basis of an extremal principle [34].

The phase diagram as function of the boundary rates α and β has a generic structure. The number of phases observed depends only on the number of local maxima in the fundamental diagram. For generic traffic systems it has only one maximum and the α - β -phase diagram consists of three phases, the high-density phase (HD), the low-density phase (LD) and the maximum current phase (MC), see Figure 9. When the supply rate α of the particles is larger than the removal rate β and $\beta < \beta_c$, the particle extraction is the limiting process resulting in

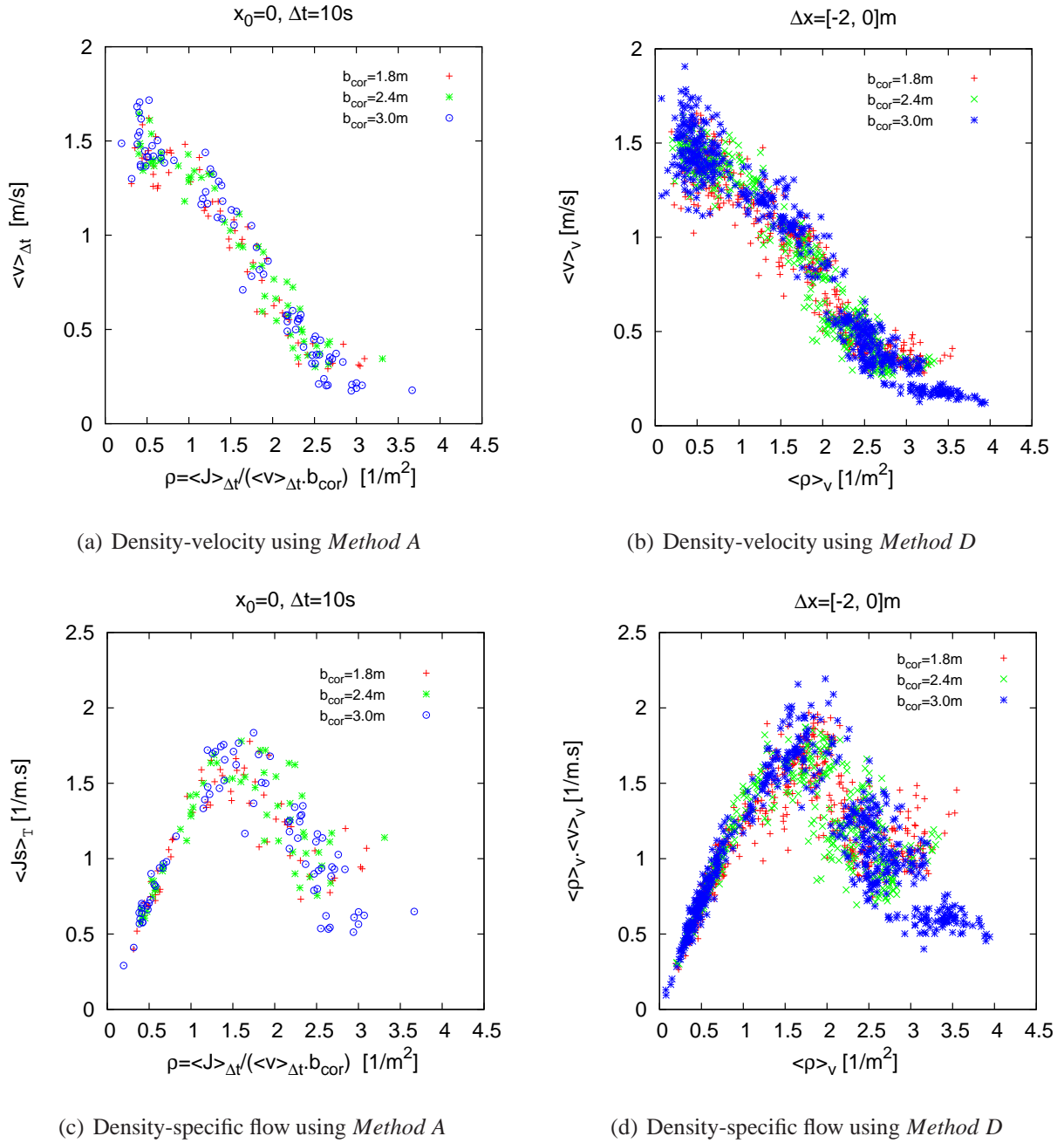


Figure 7. Comparison of the fundamental diagram in different corridor widths.

a high density phase where the current is independent of α . When the particles are supplied not too fast, $\alpha < \alpha_c$ and $\beta > \alpha$, a low density phase is formed which is limited by particle supply. Here the current is independent of α . There is a discontinuous phase transition along the line $\alpha = \beta < \alpha_c$. When particles are supplied and removed sufficiently rapidly, $\alpha > \alpha_c$ and $\beta > \beta_c$, a continuous phase transition into a maximum-current phase for which transport is bulk dominated [32] occurs where the current is independent of both α and β .

The experiments in the corridor geometry can effectively be described by such a scenario. The input rate α into the corridor is controlled by the width b_{entrance} of the entrance whereas

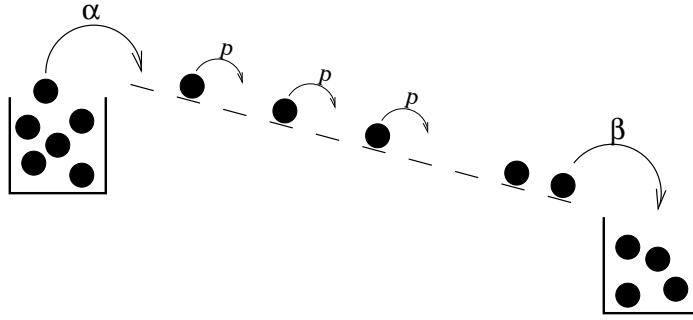


Figure 8. Open system with particle input at the left boundary with rate α and particle output at the right boundary with rate β .

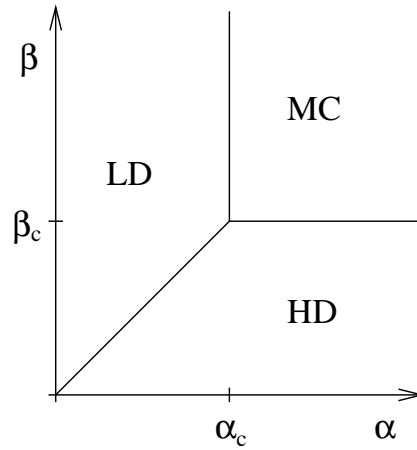


Figure 9. Generic form of the phase diagram for an open system with input rate α and output rate β . In the LD phase the current has the form $J = J(\alpha; p)$ and in the HD phase $J = J(\beta; p)$. In the MC phase, the current is independent of α and β and corresponds to the maximum of the fundamental diagram: $J = J_{\max}(p)$.

the output rate β is controlled by the width b_{exit} of the exit. Therefore the α - β -phase diagram corresponds in our case to a b_{entrance} - b_{exit} -diagram. The width b_{cor} of the corridor, on the other hand, controls the maximal possible bulk flow in the system, given by the maximal flow J_{\max} in the fundamental diagram.

For the experiments with $b_{\text{exit}} = b_{\text{cor}}$ the flow through the system is not limited by the exit (see Fig. 6), corresponding to the case $\beta > \beta_c$. The system is then in the low-density phase. Here the flow is controlled by the inflow into the system, i.e. effectively by b_{entrance} . At $b_{\text{entrance}} \approx 1.45$ m a transition into the maximum current phase can be observed (see especially Fig. 6(a)). For $b_{\text{entrance}} = b_{\text{cor}}$ and $b_{\text{exit}} < b_{\text{cor}}$ the system is in the high-density phase. The phase diagram will be investigated in more detail in a separate publication [35].

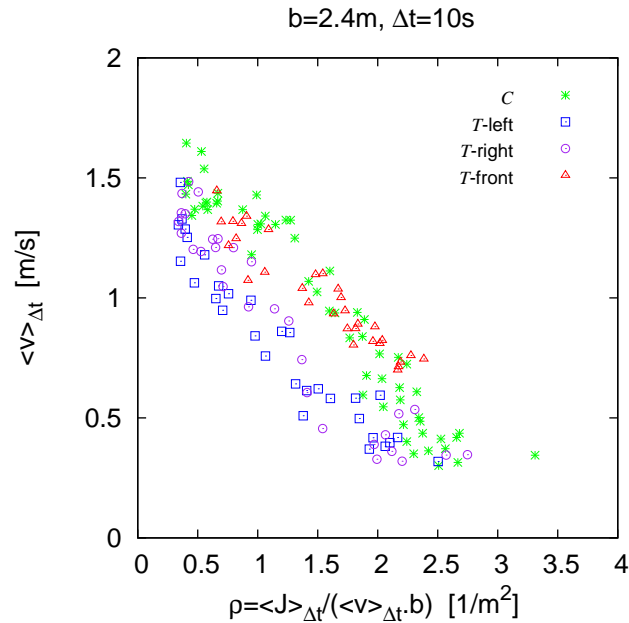


Figure 10. Comparison of the fundamental diagrams between straight corridor and T-junction

4.5. Comparison of straight corridor with T-junction

In this section, we compare the fundamental diagrams for a straight corridor (C) and T-junction (T) with channel width $b = 2.4$ m.

Figure 10 shows the results obtained from the experiments C and T using *Method A*. The data assigned with 'T-left' and 'T-right' are measured in the area before the stream merge (see Figure 1(c)). The data assigned with 'T-front' are measured in the region where the streams already merged. The comparison shows that the fundamental diagram of the unidirectional flow agrees with the fundamental diagram of the T-junction in the 'front' part (T -front). But for the density region ρ from 0.5 m^{-2} to 2 m^{-2} the velocities at the 'right' and 'left' part of the T-junction (T -left and T -right) are significantly lower. For densities higher than 2 m^{-2} the difference is smaller. The differences in the fundamental diagram could be interpreted in the following way. The dynamics in the region after the merging of the streams is comparable with the unidirectional pedestrian flow in an open corridor. But in front of the merging the velocities are significantly lower indicating that the dynamics of the stream changes due to the change of the geometry and the merging of the streams.

5. Summary

Series of well-controlled laboratory pedestrian experiments were performed in straight corridors and T-junction in this study. Up to 350 persons participated in these activities and the whole processes of the experiment were recorded using two video cameras. The trajectories of each pedestrian are extracted with high accuracy from the video recordings automatically using *PeTrack*. Four measurement methods are adopted in this study and their

influences on the fundamental diagram are investigated. It is found that the results obtained from different methods agree well and the main differences are the range of the fluctuations and the resolution in time of the results. The influence of the corridor width on the results is also investigated. It is shown that fundamental diagrams for the same type of facility but different widths agree well and can be unified in one diagram for specific flow. From the comparison of the fundamental diagrams between straight corridor and T-junction, it is indicated that the fundamental diagrams for different facilities are not comparable. The reason for this difference may be the equilibration between the inflow and outflow of pedestrians in the corridor. When the outflow and the inflow are not equal, a transition between low and high densities appears in the pedestrian flow. This transition can also be observed in the fundamental diagram.

References

- [1] C. Appert-Rolland, F. Chevoir, P. Gondret, S. Lassarre, J.-P. Lebacque, and M. Schreckenberg. *Traffic and Granular Flow '07*. Springer, Berlin Heidelberg, 2009.
- [2] S. Bandini, S. Manzoni, H. Umeo, and G. Vizzari. *Cellular Automata: 9th International Conference on Cellular Automata for Research and Industry*. ACRI 2010 Ascoli Piceno, Italy, 2010.
- [3] W. Klingsch, C. Rogsch, A. Schadschneider, and M. Schreckenberg. *Pedestrian and Evacuation Dynamics 2008*. Springer-Verlag Berlin Heidelberg, 2010.
- [4] A. Schadschneider and A. Seyfried. “Empirical Results for Pedestrian Dynamics and their Implications for Cellular Automata Models,” in *Pedestrian Behavior: Data Collection and Applications*, 1st ed., ch. 2, pp. 27–43, 2009.
- [5] A. Schadschneider, H. Klüpfel, T. Kretz, and C. Rogsch and A. Seyfried. “Fundamentals of Pedestrian and Evacuation Dynamics,” in Bazzan and Klügl (Eds) *Multi-Agent Systems for Traffic and Transportation Engineering*, USA, ch. 6, pp. 124–154, 2009.
- [6] A. Schadschneider, D. Chowdhury and K. Nishinari. “Stochastic Transport in Complex Systems - From Molecules to Vehicles,” Elsevier, 2010
- [7] A. Schadschneider, W. Klingsch, H. Kluepfel, T. Kretz, C. Rogsch, and A. Seyfried. Evacuation Dynamics: Empirical Results, Modeling and Applications, in *Encyclopedia of Complexity and System Science*. vol. 5, pp. 3142–3176, 2009.
- [8] A. Seyfried, O. Passon, B. Steffen, M. Boltes, T. Rupperecht, and W. Klingsch. “New insights into pedestrian flow through bottlenecks,” *Transportation Science*, vol. 43, pp. 395–406, 2009.
- [9] S. P. Hoogendoorn and W. Daamen, “Pedestrian Behavior at Bottlenecks,” *Transportation Science*, vol. 39, no. 2, pp. 147–159, 2005.
- [10] T. Kretz, A. Grünebohm, and M. Schreckenberg, “Experimental study of pedestrian flow through a bottleneck,” *J. Stat. Mech.*, vol. 10, p. P10014, 2006.
- [11] T. Kretz, A. Grünebohm, M. Kaufman, F. Mazur, and M. Schreckenberg, “Experimental study of pedestrian counterflow in a corridor,” *J. Stat. Mech.*, vol. 10, p. P10001, 2006.
- [12] M. Moussaïd, D. Helbing, S. Garnier, A. Johansson, M. Combe, and G. Theraulaz, “Experimental study of the behavioural mechanisms underlying self-organization in human crowds.” *Proc. R. Soc. B*, vol. 276, no. 1668, pp. 2755–2762, 2009.
- [13] X. Liu, W. Song, and J. Zhang, “Extraction and quantitative analysis of microscopic evacuation characteristics based on digital image processing,” *Physica A: Statistical Mechanics and its Applications*, vol. 388, no. 13, pp. 2717–2726, 2009.
- [14] A. Johansson, “Constant-net-time headway as a key mechanism behind pedestrian flow dynamics,” *Phys. Rev. E*, vol. 80, 026120, 2009.

Table 2. Parameters for the straight corridor experiments

Experiment index	Name	b_{entrance} [m]	b_{cor} [m]	b_{exit} [m]	N
1	C-050-180-180	0.50	1.80	1.80	61
2	C-060-180-180	0.60	1.80	1.80	66
3	C-070-180-180	0.70	1.80	1.80	111
4	C-100-180-180	1.00	1.80	1.80	121
5	C-145-180-180	1.45	1.80	1.80	175
6	C-180-180-180	1.80	1.80	1.80	220
7	C-180-180-120	1.80	1.80	1.20	170
8	C-180-180-095	1.80	1.80	0.95	159
9	C-180-180-070	1.80	1.80	0.70	148
10	C-065-240-240	0.65	2.40	2.40	70
11	C-080-240-240	0.80	2.40	2.40	118
12	C-095-240-240	0.95	2.40	2.40	108
13	C-145-240-240	1.45	2.40	2.40	155
14	C-190-240-240	1.90	2.40	2.40	218
15	C-240-240-240	2.40	2.40	2.40	246
16	C-240-240-160	2.40	2.40	1.60	276
17	C-240-240-130	2.40	2.40	1.30	247
18	C-240-240-100	2.40	2.40	1.00	254
19	C-080-300-300	0.80	3.00	3.00	119
20	C-100-300-300	1.00	3.00	3.00	100
21	C-120-300-300	1.20	3.00	3.00	163
22	C-180-300-300	1.80	3.00	3.00	208
23	C-240-300-300	2.40	3.00	3.00	296
24	C-300-300-300	3.00	3.00	3.00	349
25	C-300-300-200	3.00	3.00	2.00	351
26	C-300-300-160	3.00	3.00	1.60	349
27	C-300-300-120	3.00	3.00	1.20	348
28	C-300-300-080	3.00	3.00	0.80	270

Table 3. Parameters for the T-junction experiments

Experiment index	Name	b_{cor1} [m]	b_{entrance} [m]	b_{cor2} [m]	N
1	T-240-050-240	2.40	0.50	2.40	134
2	T-240-060-240	2.40	0.60	2.40	132
3	T-240-080-240	2.40	0.80	2.40	228
4	T-240-100-240	2.40	1.00	2.40	208
5	T-240-120-240	2.40	1.20	2.40	305
6	T-240-150-240	2.40	1.50	2.40	305
7	T-240-240-240	2.40	2.40	2.40	302

- [15] A. Johansson and D. Helbing, "From crowd dynamics to crowd safety: a video-based analysis," *Advances in Complex Systems (ACS)*, vol. 4, no. 4, pp. 497–527, 2008.
- [16] S. B. Young, "Evaluation of Pedestrian Walking Speeds in Airport Terminals," *Transportation Research Record*, vol. 1674, pp. 20–26, 1999.
- [17] J. J. Fruin. *Pedestrian Planning and Design*. Elevator World, New York, 1971.
- [18] V. M. Predtechenskii and A. I. Milinskii. *Planning for Foot Traffic Flow in Buildings*. Amerind Publishing, New Delhi, 1978, translation of: Proekttirovanie Zhdanii s Uchetom Organizatsii Dvizheniya Lyudskikh Potokov, Stroizdat Publishers, Moscow, 1969.
- [19] U. Weidmann. "Transporttechnik der Fussgänger," Schriftenreihe des Institut für Verkehrsplanung, Transporttechnik, Strassen- und Eisenbahnbau, ETH Zürich, 1993), Vol. 90.
- [20] D. Helbing, A. Johansson, and H. Z. Al-Abideen, "Dynamics of Crowd Disasters: An Empirical Study," *Physical Review E*, vol. 75, p. 046109, 2007.
- [21] A. Seyfried, M. Boltes, J. Kähler, W. Klingsch, A. Portz, T. Rupperecht, A. Schadschneider, B. Steffen, and A. Winkens. "Enhanced empirical data for the fundamental diagram and the flow through bottlenecks," in *Pedestrian and Evacuation Dynamics 2008*. Springer-Verlag Berlin Heidelberg, pp. 145–156, 2010.
- [22] U. Chattaraj, A. Seyfried, and P. Chakroborty. "Comparison of Pedestrian Fundamental Diagram Across Cultures," *Advances in Complex Systems (ACS)*, vol. 12, no. 3, pp. 393–405, 2009.
- [23] F. D. Navin and R. J. Wheeler. "Pedestrian flow characteristics," *Traffic Engineering*, vol. 39, pp. 31–36, 1969.
- [24] B. Pushkarev and J. M. Zupan. "Capacity of Walkways," *Transportation Research Record*, vol. 538, pp. 1–15, 1975.
- [25] B. D. Hankin and R. A. Wright. "Passenger Flow in Subways," *Operational Research Quarterly*, vol. 9, pp. 81–88, 1958.
- [26] <http://www.fz-juelich.de/jsc/hermes>
- [27] M. Boltes, A. Seyfried, B. Steffen, and A. Schadschneider. "Automatic Extraction of Pedestrian Trajectories from Video Recordings," in *Pedestrian and Evacuation Dynamics 2008*. Springer-Verlag Berlin Heidelberg, pp. 43–54, 2010.
- [28] W. Leutzbach. *Introduction to the Theory of Traffic Flow*. Springer, 1988.
- [29] B. S. Kerner. *The Physics Of Traffic: Empirical Freeway Pattern Features, Engineering Applications, and Theory*, 1st ed., J. A. S. Kelso, Ed. Springer, 2004.
- [30] B. Steffen and A. Seyfried. "Methods for measuring pedestrian density, flow, speed and direction with minimal scatter," *Physica A*, vol. 389, no. 9, pp. 1902–1910, 2010.
- [31] G. M. Voronoi. "Nouvelles applications des paramètres continus à la théorie des formes quadratiques," *Journal für die reine und angewandte Mathematik*, vol. 133, pp. 198–287, 1908.
- [32] J. Krug. "Boundary-Induced Phase Transition in Driven Diffusive Systems," *Phys. Rev. Lett.*, vol. 67, no. 14, pp. 1882–1885, 1991.
- [33] A. Kolomeisky, G. Schütz, E. Kolomeisky, and J. Straley. "Phase diagram of one-dimensional driven lattice gases with open boundaries," *J. Phys. A*, vol. 31, pp. 6911–6919, 1998.
- [34] V. Popkov and G. Schütz. "Steady-state selection in driven diffusive systems with open boundaries," *Europhys. Lett.*, vol. 48, no. 3, pp. 257–263, 1999.
- [35] J. Zhang, A. Schadschneider and A. Seyfried. "in preparation,"